

## Original Study

**Cite this article:** Vorobyov MS, Koval TV, Koval NN, Hung NB (2018). Generation, transport, and efficient extraction of a large cross-section electron beam into an air in an accelerator with a mesh plasma cathode. *Laser and Particle Beams* **36**, 22–28. <https://doi.org/10.1017/S0263034617000969>

Received: 2 October 2017  
Accepted: 10 December 2017

**Key words:**

Electron accelerator; large cross-section electron beam in air; mesh stabilization; plasma cathode

**Author for correspondence:**

Maxim S. Vorobyov, Institute of High Current Electronics, Tomsk 634055, Russia. E-mail: [vorobyovms@yandex.ru](mailto:vorobyovms@yandex.ru)

# Generation, transport, and efficient extraction of a large cross-section electron beam into an air in an accelerator with a mesh plasma cathode

Maxim S. Vorobyov<sup>1</sup>, Tamara V. Koval<sup>2</sup>, Nikolay N. Koval<sup>1,2</sup> and Nguyen Bao Hung<sup>2</sup>

<sup>1</sup>Institute of High Current Electronics, Tomsk 634055, Russia and <sup>2</sup>National Research Tomsk Polytechnic University, Tomsk 634050, Russia

**Abstract**

The paper presents experimental and theoretical research data on the generation, transport, and extraction of a large cross-section ( $750 \times 150 \text{ mm}^2$ ) electron beam into the air through a thin metal foil in an accelerator with a mesh plasma cathode on the bases of a low-pressure arc and with a multi-aperture two-electrode electron-optical system. When the burning conditions of the arc discharge, responsible for the generation of the emission plasma, is changed, the characteristics of this plasma were investigated, including under the conditions of the selection of electrons from it. Our experiments show that at an accelerating voltage of 200 kV, current in the accelerating gap of up to 30 A, and full width at half maximum of up to 100  $\mu\text{m}$ , the average extracted power is  $\approx 4 \text{ kW}$  and the extracted beam current is  $\approx 85\%$  from the common current into the accelerating gap. Our numerical estimates give a good correlation between the arc and emission plasma parameters depending on the electrode configuration in the discharge system and on the mechanism of electron beam generation. Analysis of the emission plasma parameters under different arc conditions and of the mechanisms responsible for the beam energy loss suggests that most of the energy in the accelerator is lost at the support grid and at the output foil due to defocusing of the beam and partial electron reflection from the foil. Other mechanisms that decrease the extracted beam energy are discussed.

**Introduction**

Electron beams of the large cross-section ( $10^2\text{--}10^4 \text{ cm}^2$ ) extracted through foil windows into the air or high-pressure gas are used for excitation of high-power lasers, polymerization of monomers, switching of high currents, sterilization of foodstuffs and medical tools, air and water purification, plasma chemistry, radiation chemistry, and so on. (James, 1979; Bugaev *et al.*, 1984; Sokovnin, 2007; Vorob'ev *et al.* 2015]. Often, one of the major problems in sources of such beams is to minimize the energy loss of a beam during its formation, transport, and extraction.

The Institute of High Current Electronic SB RAS (Tomsk, Russia) develops electron sources based on a low-pressure arc with a mesh plasma cathode (Gielkens *et al.*, 1996; Grigoryev *et al.*, 2008; Vorob'ev *et al.*, 2014; Vorobyov *et al.*, 2015a, b, c) which find application in unique facilities of Russia [<http://ckp-rf.ru/usu/434216>]. The use of the arc discharge for the generation of emission plasma provides high energy efficiency of such electron sources as the average discharge power is no greater than 100 W at an average beam power of up to several kilowatts, and the mesh-stabilized emission boundary allows one to independently control the beam parameters (electron energy, beam current, pulse repetition frequency) and vary them over a wide range.

Here we present experimental and theoretical data on the plasma characteristics, electron beam parameters, and main energy loss mechanisms in a wide-aperture electron accelerator based on a low-pressure arc with a mesh plasma cathode.

**Experimental setup and measurement methods**

The generation, transport, and an electron beam extraction into the air were studied on an accelerator with a multi-aperture mesh plasma cathode based on the low pressure arc (Vorobyov *et al.*, 2015a, b, c). Its simplified schematic and photo are presented in Figures 1 and 2, respectively. The accelerator provides the formation of a cross-section electron beam ( $750 \times 150 \text{ mm}^2$ ) in repetitive pulsed modes with the following maximum beam parameters (not at the same time): electron

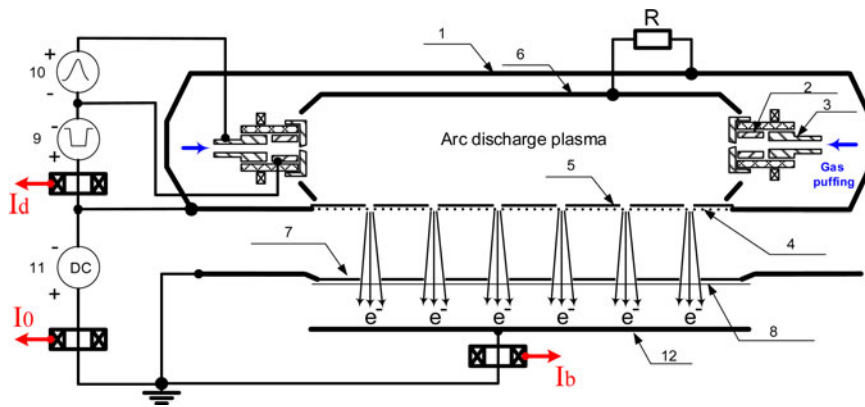


**Fig. 1.** Schematic of the electron accelerator: 1 – plasma cathode; 2 – metal cathode; 3 – igniter; 4 – emission mesh; 5 – mask; 6 – hollow anode; 7 – support grid for output foil; 8 – output foil; 9 – discharge power supply; 10 – igniter power supply; 11 – high-voltage power supply; 12 – collector or substrate.

energy 200 keV, beam current in air 30 A, pulse duration 100  $\mu$ s, and pulse repetition frequency 50 Hz.

In the accelerator (Fig. 1), plasma cathode 1 is a hollow stainless steel semi-cylinder of dimensions  $200 \times 150 \times 800$  mm<sup>3</sup> at the ends of which there are two cathode units based on a low-pressure arc with a cathode spot initiated by an electrical breakdown of the working gas (Vorobyov *et al.*, 2015a, b, c).

The inner surface of the semi-cylinder serves as hollow anode 6 for two cathode units. Emission mesh 4 of dimensions  $750 \times 150$  mm<sup>2</sup> is covered with stainless steel mask 5 of thickness 200  $\mu$ m (Fig. 3a) having 344 holes of diameter 8–12 mm. Each section of the mesh bounded by a hole in the mask is individual emission elements of the mesh plasma cathode. Hollow anode 6 is connected to emission mesh 4 via resistance *R* to provide switching of the discharge current to the emission region. For electron extraction from the emission surface, an accelerating dc voltage of up to  $U_0 \leq 200$  kV is applied between the plasma cathode 1 and output foil window 7,8 of the accelerator. The accelerating gap is  $d = 140$  mm. The output foil window (Fig. 3b) comprises support Cu grid 7 of thickness 20 mm and output Al–Mg foil 8 of thickness 30  $\mu$ m which provides extraction of electrons with energies  $E_0 \geq 80$  keV (Seltser & Berger, 1974). The support grid has a total geometric transparency of 56%. The number of coaxial holes in the support grid is the same as that in the mask but their diameter is larger (15 mm). Thus, the broad electron beam represents a superposition of elementary beams formed by individual emission elements whose plasma boundary is stabilized by the fine metal mesh.



**Fig. 2.** DUET electron accelerator.

The discharge current  $I_d$ , current in the accelerating gap  $I_0$ , and beam current  $I_b$  extracted into the air were measured with Rogowski coils in the respective circuits (Fig. 1). The beam current  $I_b$  was measured with Al collector 12 of dimensions  $800 \times 200$  mm<sup>2</sup> located in the air at 20 mm from the output foil.

### Experimental and theoretical research

The multi-aperture two-electrode electron-optical system has allowed us to increase the accelerator efficiency by increasing the beam extraction factor  $\beta = I_b/I_0$ . Of significance is that our estimates of  $I_b$  (Fig. 4a) take into account the reflection of accelerated electrons from the collector, as opposed to data reported elsewhere (Vorobyov *et al.*, 2015a, b, c). Decreasing the beam current loss has made it possible to increase the average output beam power from 2.5 kW to more than 4 kW and thus to bring the accelerator to a new technological level. The further increase in the average beam power was limited by the maximum output power of the high-voltage power supply.

Previously (Vorobyov *et al.*, 2015a, b, c), it was also reported that decreasing the mask hole diameter, that is, the electron emission area, can provide higher values of  $\beta$  and more stable operation of the mesh plasma cathode. However, this decreases the electron extraction factor  $\alpha = I_0/I_d$ . As can be seen from Figure 4b, the factor  $\alpha$  depends on the accelerating voltage  $U_0$  and on the emission plasma density  $n_e$  which increases with  $I_d$ . It is also obvious that  $\alpha$  increases with  $h$ . Based on the work of (Oks, 2006) let us consider these phenomena at greater length.

For analyzing the discharge plasma characteristics (plasma density, electron temperature, plasma potential), we can use a

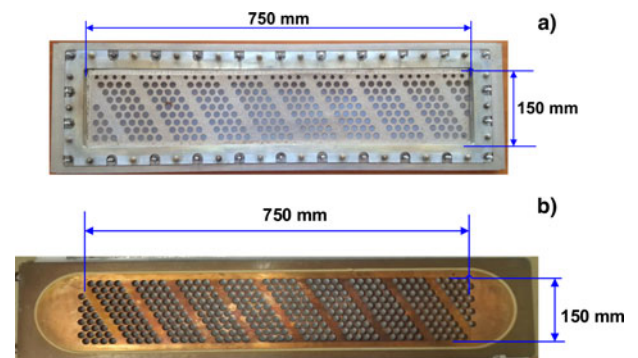


**Fig. 3.** Spot-welded mask on emission mesh (a) and output foil window (b).

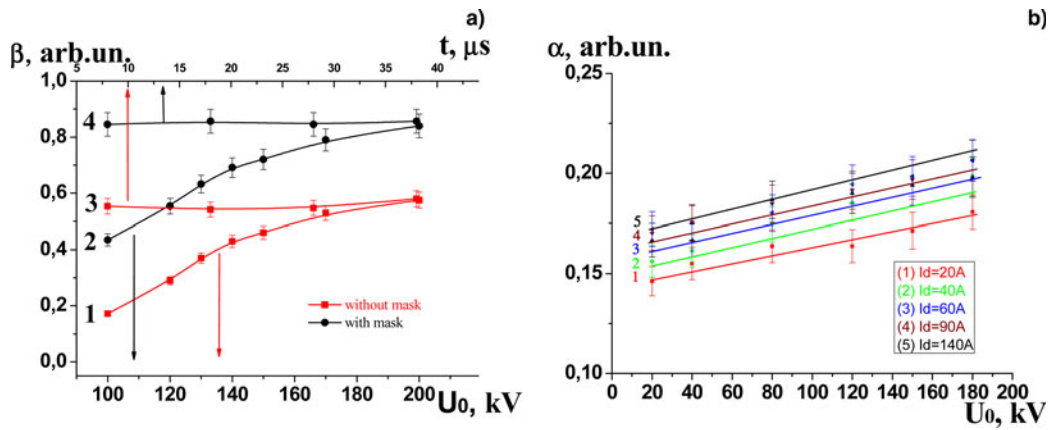


**Fig. 4.** Beam extraction efficiency  $\beta$  versus accelerating voltage  $U_0$  and beam pulse duration  $t$  at  $U_0 = 200$  kV (a) with no mask (1, 3) and with it (2, 4) and electron extraction efficiency  $\alpha$  versus  $U_0$  with mask holes of diameter 8 mm and mesh width  $h = 0.6$  mm (b).

numerical model which describes the density of plasma electrons  $n_e = n_i$  and their average energy  $n_e$  as a function of space and time (Hagelaar & Pitchford, 2005):

$$\frac{\partial n_{e,\varepsilon}}{\partial t} + \nabla \vec{\Gamma}_{e,\varepsilon} = R_{e,\varepsilon}, \quad \vec{\Gamma}_{e,\varepsilon} = -D_{e,\varepsilon} \cdot \nabla n_{e,\varepsilon}. \quad (1)$$

here  $\Gamma_{e,\varepsilon}$  is the electron and energy flux;  $\mu_{e,\varepsilon}$  is the electron mobility and energy;  $D_{e,\varepsilon}$  is the diffusion coefficient; and  $R_{e,\varepsilon}$  is the rate of ionization and change of electron energy due to inelastic collisions dependent on the electron energy distribution function. Model (1) ignores the processes in the collisionless electric double layer between the discharge column and target; the input data (electron flux and energy) are determined from experiments. The plasma potential with respect to the emission electrode is estimated by the formula:

$$\varphi = \frac{kT_e}{e} \cdot \ln\left(2 \frac{1+r}{1-r}\right), \quad (2)$$

where  $k$  is Boltzmann's constant,  $e$  and  $T_e$  are the electron charge and its temperature,  $r$  is the electron reflection coefficient from the computational domain boundary.

As the experiment suggests, increasing the resistance  $R$  decreases the current rise time in the accelerating gap such that at  $R \geq 10 \Omega$  the current  $I_0$  takes a more stable shape with a clearer

flat peak, reproducing the discharge current  $I_d$ . The effect of  $R$  on the discharge plasma parameters was analyzed numerically using model (1) with  $R$  taken as the electron reflection coefficient  $r$  from the anode surface and with the electron current to the anode cavity  $I_a(r)$  corresponding to experimental  $I_a(R)$ .

For the total mesh transparency  $\approx 45\%$  (cell width  $h = 0.4$  mm) without mask 5 (Fig. 1), the electron extraction factor  $\alpha$  from the plasma cathode to the accelerating gap of width  $d = 140$  mm reaches its maximum value at  $R \geq 10 \Omega$  in the anode circuit (Fig. 5a) and remains almost constant with further increasing the resistance  $R$ . As already noted, the factor  $\alpha$  increases with increasing the discharge current and accelerating voltage, which is due to a penetration of the electric field from the accelerating gap to the space of the plasma cathode through cells of the emission mesh when the electron component of the discharge current takes the path through the circuit of the high-voltage power supply (Oks, 2006). From Figure 5a it is seen that this method of current switching is very efficient and provides a near two-fold increase in the electron extraction factor  $\alpha$  for almost no change in the discharge operating voltage  $U_d$  (Fig. 5b).

Figure 6 presents experimental curves for the hollow anode current  $I_a$  as a function of  $R$  and calculated curves for the plasma density  $n_e$  and plasma potential  $\varphi$  with respect to the anode at  $I_d = 100$  A and  $I_d = 20$  A. The calculations show that increasing the resistance  $R$  from 0 to 10  $\Omega$  allows to increase the plasma density  $n_e$  and plasma potential  $\varphi$ . This is because the fraction

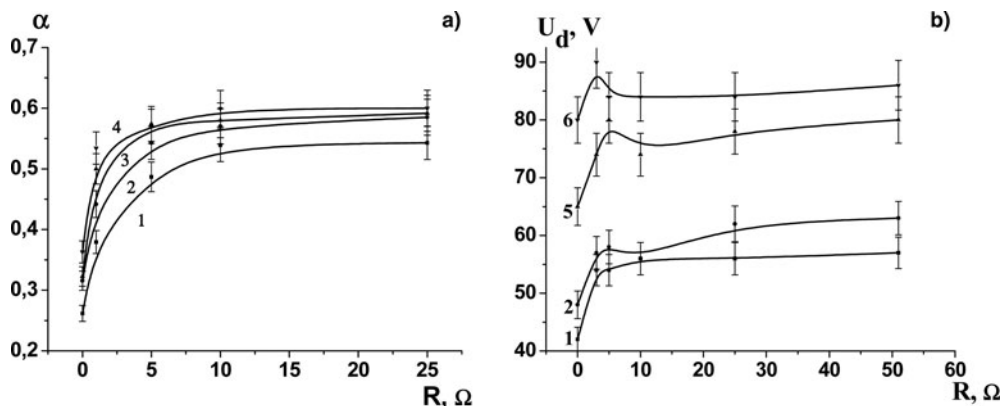


**Fig. 5.** Electron extraction factor  $\alpha$  (a) and discharge operating voltage  $U_d$  (b) versus resistance  $R$  in experiments with no mask at  $U_0 = 160$  kV,  $h = 0.4$  mm, and  $d = 140$  mm for  $I_d$  equal to 20 A (1), 40 A (2), 60 A (3), 90 A (4), 100 A (5), and 150 A (6).

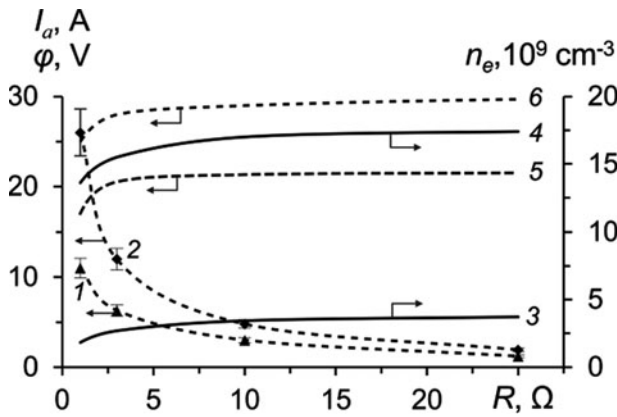


Fig. 6. Experimental curves for anode current  $I_a$  (1, 2) and respective calculated curves for plasma density  $n_e$  (3, 4) and plasma potential  $\phi$  (5, 6) with respect to anode as a function of  $R$  at  $I_d = 20$  A (1, 3, 5) and 100 A (2, 4, 6).

of electrons reflected from hollow anode walls increases, the number of their interactions with the working gas grows, and this increases the density of chaotic current and hence the emission current.

From the calculations, it follows that the saturation of  $\alpha$  at  $R > 10 \Omega$  (Fig. 5a) is most likely due to near-total reflection of plasma electrons from the anode. The continuity of the current, in this case, is provided by fast electrons which are accelerated in the region of cathode potential fall and reach the hollow anode with minimum energy loss.

Thus, the discharge current in the plasma cathode is determined by the following components: the current of fast electrons  $I_{eb}$  not participating in the gas ionization into the plasma cathode, the electron current to the metal surface of the hollow anode and emission mesh, and the emission current through the potential barrier  $\Delta\phi = \phi_f(r) - DU_0(z_{pl})$  (Oks, 2006):

$$I_d = I_{eb} + j_{ch} S_a \ell \frac{e\phi}{kT_e} + j_{ch} S_f \ell \frac{e\phi_f}{kT_e} + j_{ch} S_e \ell \frac{e\Delta\phi}{kT_e}. \quad (3)$$

Here  $S_a$  and  $S_f$  are the metal surface areas of the hollow anode and emission mesh;  $S_e$  is the cell area of the emission mesh;  $\phi_f$  is the plasma potential with respect to the emission electrode;  $U_0$  is the accelerating voltage in the diode;  $j_{ch}$  is the chaotic current density;  $DU_0(z)$  is the accelerating field which penetrates in the plasma cathode through mesh cells and is approximated by the formula:

$$DU_0(z) = c_1 \frac{hU_0}{2d} \exp\left(-2c_2 \frac{\rho - z}{h}\right). \quad (4)$$

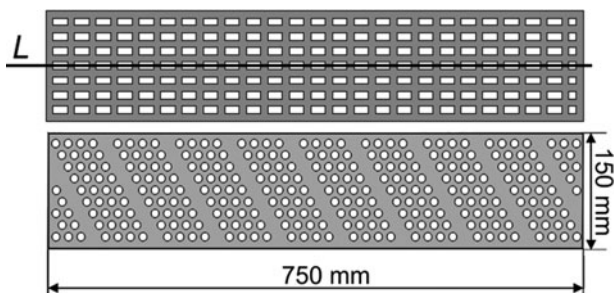


Fig. 7. Mask geometry in calculations and experiments.

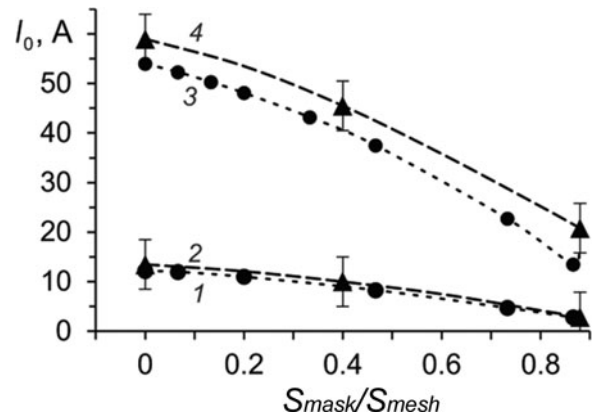


Fig. 8. Current in the accelerating gap  $I_0$  as a function of  $S_{mask}/S_{mesh}$  at  $U_0 = 200$  kV,  $h = 0.6$  mm in calculations (1, 3) and experiments (2, 4) for  $I_d = 20$  A (1, 2), 90 A (3), and 100 A (4).

Here  $D$  is the coefficient of electrical permeability of the emission electrode,  $c_1, c_2$  are constants dependent on the mesh transparency,  $h$  is the cell width,  $\rho$  is the mesh wire diameter, and  $d$  is the length of the accelerating gap.

Assuming for simplicity that  $I_{eb} \approx 0$  in (3), the expression for the electron extraction factor  $\alpha$  takes the form:

$$\alpha = \left[ e^{-\frac{\Delta\phi}{kT_e}} \right] \left[ \frac{S_a}{S_e} e^{-\frac{e\phi}{kT_e}} + \frac{S_f}{S_e} e^{-\frac{e\phi_f}{kT_e}} + e^{-\frac{e\Delta\phi}{kT_e}} \right]^{-1} \quad (5)$$

The plasma potential  $\phi$  and the plasma density  $n_e$  increase simultaneously with  $R$  (Fig. 6). From expressions (3) and (5) it follows that increasing the plasma potential  $\phi$  decreases the current to the hollow anode  $I_a$  and increases the current in the accelerating gap, which increases the extraction factor  $\alpha$ .

When a change occurs in the plasma potential  $\phi_f$  or in the accelerating voltage  $U_a$ , it changes the position of the plasma emission boundary. The position of the boundary is determined from the condition of equality of the electrostatic pressure in the accelerating gap  $\epsilon_0 E^2/2$  and the kinetic pressure of the plasma  $n_e kT_e$  (Oks, 2006), where  $\epsilon_0$  is the dielectric constant and  $E$  is the electric field strength in the accelerating gap, with the plane  $z_{pl} = 0$  coincident with the emission mesh plane from the side of the plasma cathode:

$$z_{pl} = \rho \left[ 1 - \frac{h}{2} c_2 \ln\left(\frac{c_1 c_2 U_0}{dE}\right) \right] \quad (6)$$

when electrons are emitted through the potential barrier ( $z_{pl} < 0$  or  $h/2 < l_i$ , where  $l_i$  is the thickness of the positive space charge layer separating the plasma from the emission electrode), the emission mesh stabilizes the plasma boundary as long as the increase in the emission current is compensated by the increase in the plasma potential, provided that  $\phi_f(r) > DU_0(z_{pl})$  and the potential  $\phi_f(r)$  does not exceed the breakdown potential (mesh electrode - discharge plasma) (Burdovitsin *et al.*, 2002; Oks, 2006; Gavrilov *et al.*, 2008; Devyatkov & Koval, 2014).

In addition, calculations were performed to study the influence of the emission surface area on the plasma parameters. For simplicity, the mask was represented as a uniform rectangular mesh

structure on the emission mesh surface (Fig. 7). Figure 8 shows experimental and calculated curves for the emission current  $I_{em}$  as a function of  $S_{mask}/S_{mesh}$ , where  $S_{mask}$  is the mask surface area and  $S_{mesh}$  is the mesh surface area. The calculations suggest that as the ratio  $S_{mask}/S_{mesh}$  is increased from 0 to 0.5, the plasma density increases by 36% with slight variations in the plasma temperature  $T_e$  and potential  $\phi_f$  and the layer thickness  $l_i$  decreases by  $\approx 15\%$ :  $l_i = r_D(e\phi_f/kT_e)^{3/4}$ , where  $r_D = (\epsilon_0 kT_e/e^2 n_e)^{1/2}$  is the Debye radius. Thus, the increase in  $R$  and the use of the mask on the mesh create an electrostatic trap which increases the number of electrons reflected from the inner walls of the hollow anode, mask, and mesh wires.

Our experiments show that without mask at  $d = 140$  mm and  $h = 0.6$  mm, the operation of the electron accelerator is unstable. The currents  $I_d$  and  $I_0$  reveal high-frequency modulations at about 1–2 MHz and the accelerating voltage starts influencing the shape and amplitude of the discharge current. This eventually decreases the electric strength of the accelerating gap (in terms of breakdowns per 1000 pulses of beam current) and the operation stability of the plasma cathode power supply up to the failure of its circuit elements. The use of a mask in the emitter eliminates all high-frequency modulations on the oscillograms of  $I_d$  and  $I_0$  and the influence of the accelerating voltage on their shape and amplitude.

Figure 9 shows typical waveforms for  $I_d$  and  $I_0$  at  $U_a = 150$  kV with mask holes of diameter 8 mm, geometric transparency 13%, and mesh width  $h = 0.6$  mm. Figure 10 presents calculation data demonstrating how the plasma density  $n_e$  varies with time  $t$  along the longitudinal axis of the plasma cathode at the emission mesh surface. Our experiments suggest that even without additional measures, for example, the use of a mask with variable geometric transparency (Vorob'ev and Koval 2016), the plasma density nonuniformity is no greater than 15% and the beam extraction factor  $\beta$  remains constant throughout the beam current pulse (see Fig. 4).

The beam current loss can be caused by the following main factors: (1) imperfect alignment of holes in the mask and support grid; (2) defocusing of the beam due to Coulomb repulsion of particles and electric field inhomogeneity in the region of emission holes; (3) scattering of electrons during their acceleration at atoms of the working gas, residual gas, and gas desorbed from the electrodes; (4) reflection of high-energy electrons from

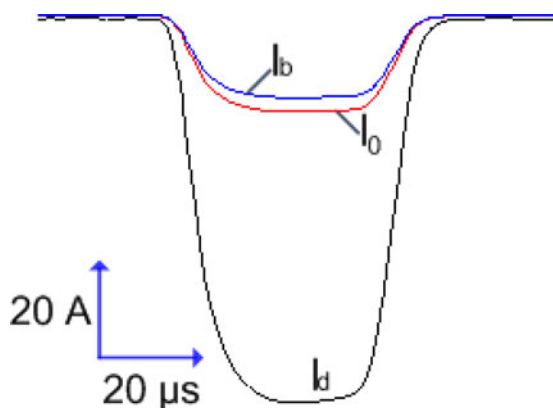


Fig. 9. Typical waveforms of discharge current  $I_d$ , current in accelerating gap  $I_0$ , and extracted beam current  $I_b$  at  $U_0 = 200$  kV with mask holes of diameter 8 mm, geometric transparency 13%, and  $h = 0.6$  mm

the output foil and their oscillation in the accelerating gap with the least probability of their escape into air but with their participation in the ionization of the working gas, residual gas, and gas desorbed from the electrodes.

The scattering of electrons at atoms of these gases leads to their ionization and to the appearance of high-energy ions in the accelerating gap, which can also be considered as a beam energy loss because ion bombardment of the plasma cathode electrodes causes their heating and decreases the overall efficiency of the accelerator. Besides, such bombardment of the emission mesh and mask brings electrons in the accelerating gap due to ion-electron emission. The number of these electrons depends on the state and material of the plasma cathode electrodes and on the energy of bombarding ions, and the probability of their escape into air is low because of the difference in electron and ion beam trajectories starting from the emission structure of the plasma cathode and from the holes of the support grid respectively (Vorobyov et al., 2015a, b, c).

Considering the balance of currents in the accelerating gap and ion-electron emission from the mask and grid surface, we analyzed the beam current loss  $I_i/I_0$  due to ion currents  $I_i = I_{ib} + I_{if}$ , where  $I_{ib}$  is the ion current due to bulk gas ionization by electrons emitted from the discharge plasma and electrons reflected from the output foil window and  $I_{if}$  is the ion current due to ionization of the gas desorbed from the foil surface by fast beam electrons whose energy corresponds to accelerating voltage.

For beam electrons with an energy of 100 keV acting on the target surface, the gas desorption is  $m = 10$  molecules/electron (Abdullin et al., 1985). The desorbed gas concentration near the target surface is  $n_{ag} = m j_0 / v_a$ , where  $v_a \approx 6 \cdot 10^4$  cm/s is the velocity of an atom. The ion current density due to bulk ionization of the gas desorbed from the foil surface by beam electrons is  $j_{if} = j_0 \sigma_{ei} d (n_g + n_{ag})$ , where  $n_g$  is the gas concentration,  $\sigma_{ei}$  is the ionization cross-section. For the electron current density in the accelerating gap  $j_0 \sim 0.1$  A/cm<sup>2</sup>, the desorbed gas concentration  $n_{ag} = 10^{14}$  cm<sup>-3</sup> is of order of magnitude higher than the working gas density in the gap  $n_g = 10^{13}$  cm<sup>-3</sup> ( $p = 0.04$  Pa). Assuming  $\sigma_{ei} \sim 5 \cdot 10^{-18}$  cm<sup>2</sup>, for example, for nitrogen (Moravej et al., 2006), the relative ion current density is  $j_{if}/j_0 \sim 5 \cdot 10^{-3}$  and its value due to bulk gas ionization by emitted and reflected electrons is  $j_i/j_0 \sim 10^{-4}$ . However, it should be noted that the ion current density increases greatly with increasing the gas pressure and electron reflection coefficient from

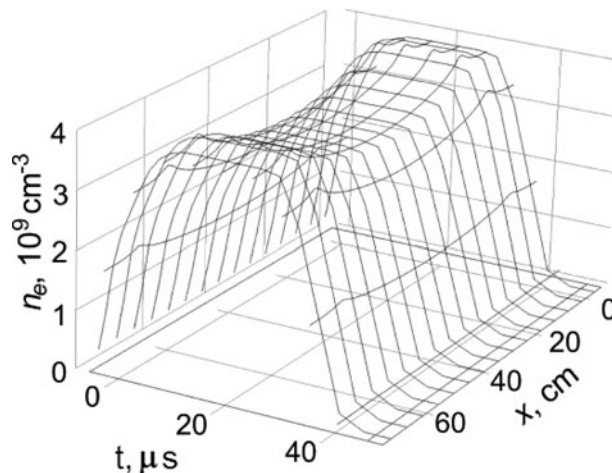
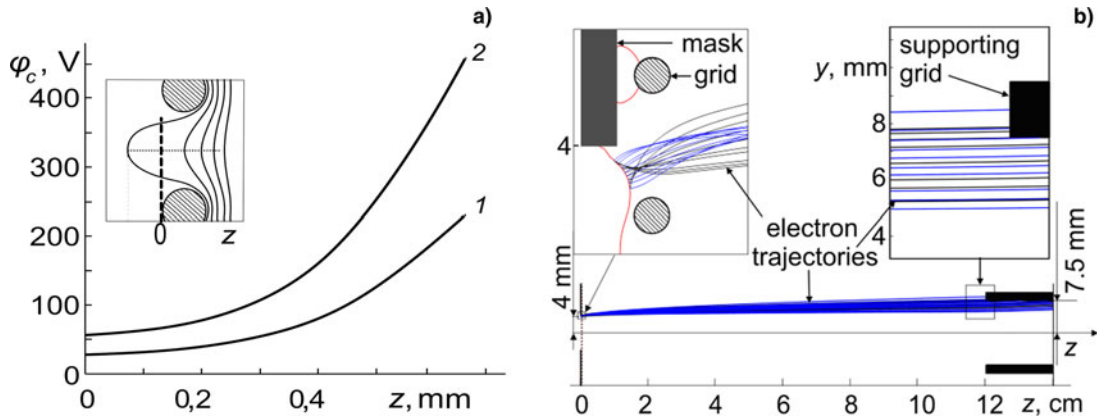


Fig. 10. Calculated variation of plasma density  $n_e$  with time  $t$  along the longitudinal axis of plasma cathode at emission mesh surface (Fig. 7, line L).



**Fig. 11.** The potential in the near-grid region due to penetration of accelerating electric field (a) at  $U_a = 100$  kV (1) and 200 kV (2), and edge effects on angular electron distribution with loose mask-to-mesh attachment (b).

the output window. Nevertheless, in our experiments, the beam current loss  $I_r/I_0$  due to ion currents is no greater than 1%.

The calculations demonstrate inessential effects of the processes associated with self-fields of elementary beams and bulk gas ionization by electrons accelerated in the diode. However, the electric field inhomogeneity in the region of emission holes (Fig. 11a) can influence the electron trajectories in the accelerating gap, eventually resulting in beam current loss at the support grid (Astrelin *et al.*, 2010). Most of the influence on the angular distribution is due to edge effects of the mask (Fig. 11b) when its coverage of end cells is incomplete and its attachment to the mesh is loose. Figure 12 shows elementary electron and ion beam configurations obtained from numerical solutions of motion equations for electron emission from the plasma boundary  $z_{pl}$  with statistically processed phase coordinates.

In experiments, the spacing between the mask and the emission mesh can reach 1 mm, causing the area of the emitting plasma surface to increase somewhat such that electrons at the

edges are angularly dispersed and fail to arrive at the support grid. Estimates show that for the spacing increased by 0.6 mm (cell width), the lost beam current can range to over 7%.

The electron and ion dynamics in the accelerating gap were studied using the PIC code KARAT (Tarakanov, 1992). Because the electric field inhomogeneity in the cell region is difficult to account for, the electrons in the emission plane were assigned initial angular and energy spreads according to the model considered above (Figs 11–12). Figure 13a shows the pattern of emitted and reflected electrons with velocity vectors (arrows) for their model distribution in the emission plane at which 10% of beam electrons with an energy of 70–150 eV have an entrance angle of  $0^\circ$ – $75^\circ$ . The loss of electrons depends strongly on their angular spread and on the mask hole diameter. For the mask hole diameter 8 mm, the beam current lost at the support grid with a hole diameter of 15 mm is  $\approx 6\%$ .

The calculations show that the loss of electrons at the support grid depends weakly on the accelerating voltage  $U_0$  due to small

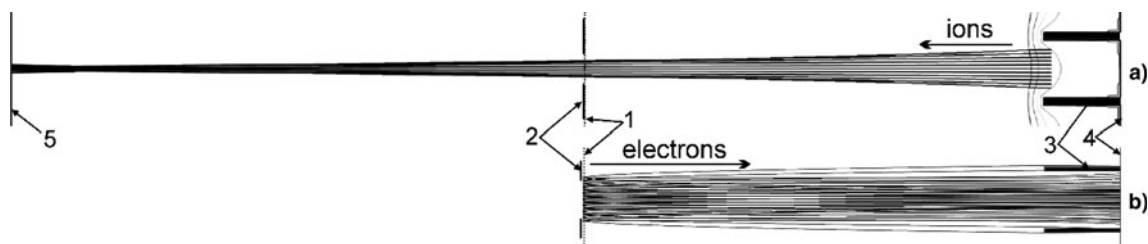


**Fig. 12.** Elementary ion (a) and electron beam configurations (b) at  $U_a = 200$  kV,  $h = 0.4$  mm, mask and support grid hole diameters 8 mm and 15 mm, respectively: 1 – emission mesh, 2 – mask, 3 – support grid, 4 – foil, 5 – discharge hollow anode.

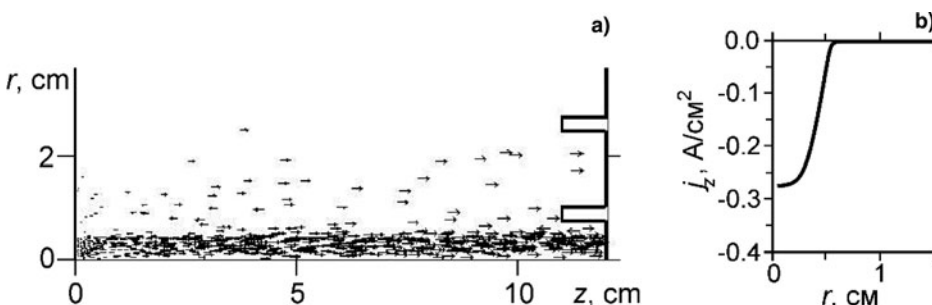


**Fig. 13.** The pattern of emitted and reflected electrons (a) and calculated current density distribution in one hole of output foil window (b).

variations in the transverse velocity of electrons arriving in the accelerating gap (Fig. 11). The main beam current losses with decreasing  $U_0$  are related to losses in the foil (Fig. 4a): the beam current in the air is  $I_b \approx 0.85 I_0$  at  $U_0 = 200$  kV and  $I_b \approx 0.6 I_0$  at  $U_a = 130$  kV, which agrees with data reported elsewhere (Seltser & Berger, 1974). According to theoretical estimates, the percent of electrons reflected from the output foil, in this case, is 3–4% of the total electron current arriving at the foil. It should be noted that the beam current loss can be contributed by a decrease in accelerating voltage during the beam current pulse and by fast electrons arising in the discharge plasma and arriving in the accelerating gap with high transverse velocities.

The two-electrode multi-aperture electron-optical system of the accelerator allows extraction of about 85% of the beam current and more than 70% of the beam power from the accelerating gap into the air (with regard to electrons reflected from the collector). The lower value of the beam power in the air compared with the beam current owes to accelerated electrons which lose part of the energy in the foil in their inelastic interactions with atoms of its lattice. In addition, the beam spends a few percent of the energy in gas heating when it passes the air gap of 2 cm between the foil and collector (Fig. 1), which also decreases the beam energy and greatly broadens its spectrum in the air (Kozyrev et al., 2015).

## Conclusion

Our experiments and numerical simulation suggest that the use of a mask in the multi-aperture plasma cathode and resistance in the hollow anode circuit makes it possible to increase the emission plasma density by more than 30% and the electron extraction efficiency by a factor  $\beta$  of  $\approx 2$  times.

According to numerical estimates, the beam current loss at the support grid depends largely on the angular velocity spread of emitted electrons which is contributed by edge effects at the mask holes, nonuniform distribution of the electric field penetrating in the plasma cathode, and fast electrons universally present in the electron energy spectrum of the discharge. The numerical estimates also show that at an operating pressure of 40 mPa and beam current density of 0.1 A/cm<sup>2</sup>, the ion fraction in the total current in the accelerating gap is no greater than 1%. Noteworthy is that for the electrons resulting from ion-electron emission, the probability of escape into the air through the foil is very low. At  $U_0 = 200$  kV, the beam current lost at the support grid can range to 7% and its loss in the output foil reaches 10%.

Elimination of the beam current loss at the support grid of the output foil window through accurate alignment of its holes with mask holes can provide a considerable increase in the efficiency and reliability of the electron accelerator, and this opens up new avenues for this type of sources in scientific and technological fields.

**Acknowledgments.** The work on this paper was supported by the Russian Science Foundation (project No. 14-29-00091).

## References

Abdullin EN, Bazhenov GP, Yerokhin GP and Ladyzhensky OB. (1985) Dynamics of growth of conductivity of an interelectrode interval in a high-voltage stage of the vacuum category. Pulse Category in Dielectrics: Novosibirsk: Science 42–55.

- Astrelin VT, Burdakov AV, Grigoriev SV, Kandaurov IV, Koval NN and Teresov AD. (2010) An influence of grid fields on beam characteristics in a diode with grid stabilization of plasma emitting surface. *Proceedings of 16th International Symposium on High Current Electronics*. Tomsk 15–18.
- Bugaev SP, Kreindel YuE and Schanin PM (1984) *Large Section Electron Beams*. Moscow: EAI.
- Burdovitsin VA, Kuzemchenko MN and Oks EM (2002) Electric strength of the accelerating gap of a plasma electron source at rough vacuum. *Technical Physics* 47(7), 926–928.
- Devyatkov VN and Koval NN (2014) Effect of electron extraction from a grid plasma cathode on the generation of emission plasma. *Journal of Physics: Conference Series* 552, 012014.
- Gavrilov NV, Emlin DR and Kamenetskikh AS (2008) Intense emission from a grid-stabilized plasma cathode. *Technical Physics* 53(10), 1308–1313.
- Gielkens SWA, Peters PJM, Witteman WJ, Borovikov PV, Stepanov AV, Tskhai VM, Zaivalov MA, Guschenets VI and Koval NN (1996) A long-pulse 300 keV electron gun with a plasma cathode for high-pressure gas lasers. *Review of Scientific Instruments* 67(7), 2449–2452.
- Grigoryev SV, Koval NN, Devyatkov VN, Teresov AD and Schanin PM. (2008) Investigation of Emission Increasing Effect at the Generation of Low-Energy Sub-Millisecond Electron Beam in the Diode with a Plasma Cathode. *Proceedings of 15th International Symposium on High Current Electronics*. Tomsk: Publishing house of the IAO SB RAS, 29–32.
- Hagelaar GJM and Pitchford LC (2005) Solving the Boltzmann equation to obtain electron transport coefficients and rate coefficients for fluid models. *Plasma Sources Science and Technology* 14, 722–733.
- James HB (1979) Electron beam sterilization technology. *Radiation Physics and Chemistry* 14, 403–414.
- Kozyrev AV, Kozhevnikov VYu, Vorobyov MS, Baksht EK, Burachenko AG, Koval NN and Tarasenko VF (2015) Reconstruction of electron beam energy spectra for vacuum and gas diodes. *Laser and Particle Beams* 33(2), 183–192.
- Moravej M, Yang X, Barankin M, Penelon J, Babayan SE and Hicks RF (2006) Properties of an atmospheric pressure radio-frequency argon and nitrogen plasma. *Plasma Sources Science and Technology* 15, 204–210.
- Oks E (2006) *Plasma Cathode Electron Sources: Physics, Technology, Applications*. WILEY-VCH.
- Seltser SM and Berger MJ (1974) The propagation and reflection of electrons by foil. *Nuclear Instruments and Methods* 119, 157–179.
- Sokovnin SYu (2007) *Nanosecond Electron Accelerators and Radiation Technologies Based on them*. Yekaterinburg: UD RAS.
- Tarakanov VP. (1992) *User's Manual for Code KARAT Springfield*. VA: Berkeley Research Associates Inc.
- Vorob'ev MS and Koval' NN (2016) Current density distribution in a large cross-section beam in an electron accelerator with a multiaperture plasma cathode. *Technical Physics Letters* 42(6), 574–576.
- Vorob'ev MS, Gameraister SA, Devyatkov VN, Koval' NN, Sulakshin SA and Shchanin PM (2014) An electron source with a multiarc plasma emitter for obtaining submillisecond pulsed megawatt beams. *Technical Physics Letters* 40(6), 526–528.
- Vorob'ev MS, Denisov VV, Koval' NN, Shugurov VV, Yakovlev VV, Uemura K and Raharjo P (2015) Radiation processing of natural latex using a wide aperture electron accelerator with a plasma emitter. *High Energy Chemistry* 49(3), 143–145.
- Vorobyov MS, Koval NN and Sulakshin SA (2015a) An electron source with a multiaperture plasma emitter and beam extraction into the atmosphere. *Instruments and Experimental Techniques* 58(5), 687–695.
- Vorobyov MS, Devyatkov VN, Koval NN and Shugurov VV (2015b) Modernization of cathode assemblies of electron sources based on low pressure arc discharge. *Journal of Physics: Conference Series* 652(1–6), 012066.
- Vorobyov MS, Koval NN, Sulakshin SA and Shugurov VV (2015c) Investigation of the stability of the electron source with a multi-aperture plasma emitter generating a large cross-section electron beam. *IOP Journal of Physics: Conference Series* 652, 012048.